NK receptors, Substance P, Ano1 expression and ultrastructural features of the muscle coat in Cav-1$^{-/-}$ mouse ileum

G. Cipriani [a], Crenguta S. Serboiu [b], Mihaela Gherghiceanu [c],
Maria Simonetta Faussone-Pellegrini [a], Maria Giuliana Vannucchi [a, *]

[a] Department of Anatomy, Histology and Forensic Medicine, Section of Histology, University of Florence, Florence, Italy
[b] 'Victor Babeş' National Institute of Pathology, Bucharest, Romania
[c] Department of Cellular and Molecular Medicine, 'Carol Davila' University of Medicine and Pharmacy, Bucharest, Romania

Abstract

Caveolin (Cav)-1 is an integral membrane protein of caveolae playing a crucial role in various signal transduction pathways. Caveolae represent the sites for calcium entry and storage especially in smooth muscle cells (SMC) and interstitial cells of Cajal (ICC). Cav-1$^{-/-}$ mice lack caveolae and show abnormalities in pacing and contractile activity of the small intestine. Presently, we investigated, by transmission electron microscopy (TEM) and immunohistochemistry, whether the absence of Cav-1 in Cav-1$^{-/-}$ mouse small intestine affects ICC, SMC and neuronal morphology, the expression of NK1 and NK2 receptors, and of Ano1 (also called Dog1 or TMEM16A), an essential molecule for slow wave activity in gastrointestinal muscles. ICC were also labelled with c-Kit and tachykinergic neurons with Substance P (SP). In Cav-1$^{-/-}$ mice: (i) ICC were Ano1-negative but maintained c-Kit expression, (ii) NK1 and NK2 receptor immunoreactivity was more intense and, in the SMC, mainly intracytoplasmatic, (iii) SP-immunoreactivity was significantly reduced. Under TEM: (i) ICC, SMC and telocytes lacked typical caveolae but had few and large flask-shaped vesicles we called *large-sized caveolae*; (ii) SMC and ICC contained an extraordinary high number of mitochondria, (iii) neurons were unchanged. To maintain intestinal motility, loss of caveolae and reduced calcium availability in Cav-1–knockout mice seem to be balanced by a highly increased number of mitochondria in ICC and SMC. Loss of Ano-1 expression, decrease of SP content and consequently overexpression of NK receptors suggest that all these molecules are Cav-1–associated proteins.

Keywords: caveolin-1 ● caveolae ● TMEM16A or ANO1 or DOG1 ● Substance P ● NK1 and NK2 receptors ● immunohistochemistry ● electron microscopy ● interstitial cells of Cajal ● smooth muscle cells

Introduction

Caveolae [1] are plasma membrane flask(omega)-shaped invaginations present in many cell types [2–4]. These structures are particularly prominent in the interstitial cells of Cajal (ICC), the gut pacemaker cells [5–9], and in the smooth muscle cells (SMC) [10, 11], but their role is not fully understood yet. In the early 1970s, caveolae were proposed as sites of excitation–contraction coupling in visceral SMC [11–13] and currently it is acknowledged the role of caveolae in smooth muscle Ca^{2+} homeostasis [14] as sites for calcium entry and storage [15, 16]. Strategic caveolae–sarcoplasmic reticulum or caveolae–mitochondria nanocontacts in SMC are probably responsible for a vectorial control of free Ca^{2+} cytoplasmic concentrations in definite nanospaces [17–20]. Caveolae have also been involved in many cellular processes: transcytosis [21, 22], potocytosis [23, 24], endocytosis [25, 26], signal transduction [27–29], control of cellular growth and proliferation [14, 28–30].

The caveolins [31–34], 21–24 kD integral proteins inserted into the inner leaflet of the plasmalemma, are the principal components of caveolae and responsible for caveolae characteristic flask shape [35]. Three caveolins isoforms have been identified: Caveolin-1, -2 and -3 (Cav-1, Cav-2 and Cav-3) [31, 32]. Cav-1 is highly

*Correspondence to: Prof. Maria Giuliana VANNUCCHI, M.D., Ph.D.,
Department of Anatomy, Histology and Forensic Medicine,
Section of Histology, University of Florence,
Viale Pieraccini, 6, 50139 Florence, Italy.
Tel.: +39-055-4271-389
Fax: +39-055-4271-385
E-mail: mariagiuliana.vannucchi@unifi.it

expressed in caveolae of the SMC and ICC. Caveolins leave both COOH- and NH$_2$-terminal ends in the cytosol where they have binding sites for numerous signalling molecules involved in the regulation and organization of various signal transduction pathways [36, 37]. In the absence of caveolins, no morphologically identifiable caveolae are detected and this loss leads to the dysfunction of caveolin-associated proteins [15, 33, 34, 37]. Recently, it has been demonstrated that either after the experimental disruption of caveolae or the genetical absence of Cav-1, as in Cav-1–knockout (Cav-1$^{-/-}$) mice, several signalling molecules are lost or dissociated from caveolins and reduced pacing frequencies and impaired contractile activity were recorded in the small intestine [15, 38–41]. Many of the molecules lacking in these animals are co-expressed with Cav-1 in both SMC and ICC and involved in Ca^{2+} handling [37]. One of these molecules is the myogenic nNOS, an enzyme modulating contraction activating L-type calcium channels [37]. Ano1 (or TMEM16A or DOG1) is a calcium-activated chloride channel involved in sensory signal transduction and smooth muscle contraction [42–45] and it is required for rhythmic contraction, as supported by the absence of slow waves in the TMEM16A knockout mice [44]. This ionic channel is expressed by the ICC [43] but whether its expression is maintained in the Cav-1$^{-/-}$ was not investigated.

In the gut of Cav-1$^{-/-}$ mice, neither the cholinergic nor the nitrergic enteric neurons are affected but the SMC show a defective responsiveness to both ACh and nitric oxide release [40, 41]. Noteworthy, the *mdx* mice, an animal model of muscular dystrophy, have a significant reduction in the caveolae number. These animals show a decrease in myogenic nNOS and NK2 receptor (NK2r) expression associated with an altered Ca^{2+} handling and a defective generation and regeneration of slow wave activity with no change in nNOS and NK1 receptor (NK1r) expression in the neurons [46–50]. To date, no information is available on possible changes in the expression of NK receptors (NKr) in the gut muscle coat of the Cav-1$^{-/-}$ mice, nor on the neurotransmitter Substance P (SP), the main NKr agonist whose interaction causes NKr internalization and smooth muscle contraction.

This study was aimed to investigate whether the absence of Cav-1 in small intestine of Cav-1$^{-/-}$ mice impairs the expression of Ano1, NKr and SP, molecules with important roles in intestinal motility. In addition, electron microscope examination was performed to identify all possible structural changes in the cell types present in the intestinal muscle coat of the Cav-1$^{-/-}$ mice.

Materials and methods

Animals and tissue collection

Specimens were obtained from the proximal part of the small intestine of six Cav-1$^{+/+}$ (B6129PF2/J) and six Cav-1$^{-/-}$ (Cav-1 KO; Cav1 tm1Mls/J) 10-week-old mice purchased from Jackson Laboratories (Bar Harbor, ME, USA). The intestine was cleaned of digestive material with saline and then cut in full thickness strips. Some of them were processed for immunohistochemistry and some others for electron microscope examination. The institutional ethical committee from 'Victor Babeş' National Institute of Pathology, Bucharest, Romania, approved this study.

Immunohistochemistry

Specimens from control and Cav-1$^{-/-}$ mice were fixed in 4% paraformaldehyde in 0.1M phosphate-buffered saline (PBS) pH 7.4, for 4–6 hrs at 4°C. Then some of them were placed in 30% sucrose in PBS, at 4°C, embedded in killik cryostat medium compound (Biooptika, Milan, Italy) and frozen at −80°C. Some other strips were dehydrated in alcohol, cleared with xylene and embedded in paraffin.

For *fluorescence and confocal microscopes examination*, 10-μm-thick transverse sections were cut with a cryostat from the frozen specimens and collected on polylysine-coated slides. The slices were pre-incubated in 5% bovine serum albumin (BSA) in PBS, pH 7.4 with 0.5% Triton X-100 for 20 min. at room temperature to minimize non-specific binding. All antisera (Cav-1, NK1r, NK2r and SP), used at different dilution, were diluted with 1% BSA with 0.5% Triton X-100 and incubated overnight at 4°C. Next day, the slices were washed for 3 × 5 min. in PBS, and then incubated for 90 min. at room temperature in a secondary antibody directed toward IgG coupled to Alexa 488 (Invitrogen, Milan, Italy) diluted at a concentration of 1:333 with BSA 1% in PBS. The sections were again washed for 3 × 2 min. in PBS and mounted in an aqueous medium (Fluoremount, Sigma, Milan, Italy). The immunoreaction products were observed under an epifluorescence Zeiss Axioskop microscope (Zeiss, Mannheim, Germany) and under a Leica TCS SP5 confocal laser scanning microscope (Leica, Mannheim, Germany) equipped with a HeNe/Ar laser source, a Leica Plan Apo 63× oil immersion objective and differential interference contrast optics. The fluorescent signal at the confocal microscope was obtained using a 488-nm excitation wavelength for the green immunofluorescence and 568 nm for the red one.

For *bright field microscope examination*, paraffin embedded sections were re-hydrated and then rinsed for 5 min. in H$_2$O$_2$ 3% and washed 3 × 5 min. in bidistilled H$_2$O. Then the sections were pre-incubated with BSA 1% in PBS for 20 min. and incubated with different antisera (Cav-1, Ano1, c-kit), used at different dilution and diluted with 1% BSA with 0.5% Triton X-100 and incubated overnight at 4°C. Next day, after washing, the sections were incubated with a secondary biotinylated antiserum (1:300 diluted in BSA 0.1% in PBS) for 2 hrs at room temperature. The sections were then washed in PBS and incubated with the ABC solution (Vector, CA, USA) for 30 min. and, after being washed with PBS, incubated with DAB (Diaminobenzidine Tables, Sigma, Milan, Italy). Finally, after washing with PBS, the sections were mounted in an aqueous medium and the immunoreactive products were observed under a Leitz light microscope (Mannheim, Germany) and photographed.

Negative controls were performed without using the primary antibodies and all of them had no labelling. All antibodies used are summarized in Table 1.

Quantitative analysis

The density of the SP-immunoreactive (SP-IR), NK1r-IR and NK2r-IR structures was evaluated in transverse sections of control and Cav-1$^{-/-}$ mouse tissue. Digitized images of 10 photographic fields of the muscle wall (four sections each animal; three animals each group, for a total of 12 sections

Table 1 Primary and secondary antibodies used

	Host	Dilution	Source	Catalogue number
Primary antibody				
NK2 receptor	Goat	1:200	Santa Cruz, CA, USA	Sc-14121
NK2 receptor	Rabbit	1:10	Gift from Grady *et al.* [52]	
NK1 receptor	Rabbit	1:500	Chemicon, Temecula, CA, USA	AB5897
NK1 receptor	Rabbit	1:100	Gift from Vigna *et al.* [51]	
Substance P	Rat	1:50	Santa Cruz, CA, USA	Sc-21715
c-kit	Rabbit	1:100	Calbiochem, San Diego, CA, USA	PC34
TMEM 16A	Rabbit	1:100	Abcam, Cambridge, MA, USA	Ab53212
Caveolin 1	Rabbit	1:200	Abcam, Cambridge, MA, USA	Ab2910
Secondary antibody				
Alexa 488 FITC	Goat	1:333	Invitrogen, San Diego, CA, USA	A-11078
Alexa 488 FITC	Rabbit	1:333	Invitrogen, San Diego, CA, USA	A-11008
Alexa 488 FITC	Rat	1:333	Invitrogen, San Diego, CA, USA	A-11006
Alexa 568 TRITC	Rat	1:333	Invitrogen, San Diego, CA, USA	A-11077
Biotinylated antibody	Rabbit	1:300	Vector, Burlingame, CA, USA	V0527

for each antibody) were acquired using at 40× objective using an AxioCam, HRm digital camera (Zeiss). Field edges were defined based on structural details within the tissue section to ensure that the fields did not overlap. All the counts were performed by two of us blind to each other. Fluorescence thresholds were set to analyse the structures of interest exclusively. These thresholds were converted to a binary image, the number of pixels above threshold was counted and the percentage area containing IR structures was calculated. The results were expressed as mean ± S.E. of the number of pixel for each image. Statistical analysis was performed by Student's *t*-test to compare two experimental groups or one-way ANOVA followed by Newman–Keuls multiple comparisons post-test when more than two groups were compared. $P < 0.05$ was considered significant.

Electron microscopy

Full-thickness strips 1 mm × 3 mm long from control and Cav-1$^{-/-}$ mice were fixed for 4 hrs at 4°C in a solution of 4% glutaraldehyde in 0.1M cacodylate buffer, pH 7.3. After four rinses in the buffer solution, the strips were post-fixed for 1 hr in 1% OsO_4 in 0.1M cacodylate buffer. After a rinse for 30 min. in distilled H_2O, the strips were dehydrated in graded ethanol and then immersed overnight in a mixture of propylene oxide and Epon 812 resin; the day after the strips were embedded in Epon 812 using flat moulds to obtain full-thickness sections with the circular muscle cut in cross-section. Semi-thin sections, obtained with an LKB-NOVA ultramicrotome, were stained with a solution of toluidine blue in 0.1M borate buffer and then observed under a light microscope. Ultra-thin sections of the selected areas were obtained by using a diamond knife and stained with a saturated solution of uranyl acetate in methanol (50:50) per 12 min. at 45°C, followed by an aqueous solution of concentrated bismuth subnitrate per 10 min. at room temperature. The sections were examined under a JEOL 1010 electron microscope (Tokyo, Japan) and photographed.

Results

Immunohistochemistry

Cav-1 immunoreactivity (IR) in controls appeared as small bars distributed along the plasma membrane on the entire cell contour (Fig. 1A). In the sections from Cav-1$^{-/-}$ mice labelled with fluorescent antibodies, this positivity was not appreciable, whereas in those labelled for bright field microscopy, Cav-1-positivity could still be detected although at a very low intensity (Fig. 1B).

c-kit-IR at the ICC located either at the myenteric plexus (MP) and deep muscular plexus (DMP) showed the same intensity and distribution in both groups of mice (Fig. 1C and D). On the contrary, the *Ano1-IR* on the ICC present in control mice (Fig. 1E) was completely lost in the Cav-1$^{-/-}$ mice (Fig. 1F).

NK1r-IR was detected either in the submucous (SMP) or MP neurons of control and Cav-1$^{-/-}$ mice with both antibodies used, that is from Vigna [51] and the commercially available one (Fig. 2A and B). SMC were also labelled by both antibodies and, in the SMC, NK1r was mainly distributed on the cell surface (Fig. 2C). The labelling was less intense with the Vigna's antibody compared with the commercially available one. Noteworthy, with the Vigna's antibody the ICC were intensely labelled (Fig. 2A). In the Cav-1$^{-/-}$ mice, immunoreactivity for NK1r was more intense with both antibodies and in the SMC it was mainly intracytoplasmatic (Fig. 2B and D).

NK2r-IR (Fig. 2E–H) distribution was identical with both antibodies used, that is from Grady *et al.* [52] and the commercially available one. In controls, the labelling was mainly distributed on
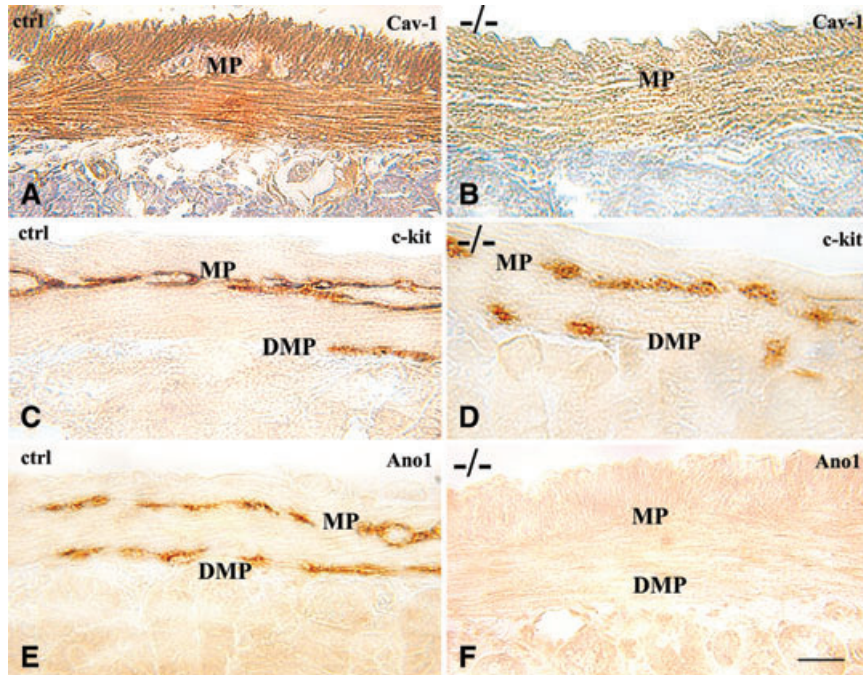
Fig. 1 (A, B) Cav-1-IR. In the control (**A**), Cav-1-IR appears as small bars distributed along the plasma membrane on the entire cell contour. In the Cav-1$^{-/-}$ mice (**B**), Cav-1-IR can be detected, although having a very low intensity. (**C**, **D**) c-kit-IR. In the control (**C**), both the ICC at the myenteric plexus (MP) and the deep muscular plexus (DMP) are c-kit-IR; in the Cav-1$^{-/-}$ mice (**D**), the c-kit-IR is perfectly maintained. (**E**, **F**) Ano1-IR. In the control (**E**), all ICC show the Ano1-IR whereas in the Cav-1$^{-/-}$ mice (**F**) these cells are Ano1-negative. Bar = 40 μm.

the plasma membrane of the SMC (Fig. 2G) whereas in the Cav-1$^{-/-}$ mice it was mostly internalized in the cytoplasm and more intense (Fig. 2F and H).

SP-IR was detected in myenteric and submucous neurons and in intragangliar and intramuscular varicose nerve fibres of control mice (Fig. 2A and E). In the Cav-1$^{-/-}$ mice, the labelled structures had the same distribution as in controls, although being significantly less numerous (Fig. 2B and F).

Quantitative analysis

The mean ± S.E.M. density of the intramuscular NK1r-, NK2r- and SP-IR was evaluated and quantitative analysis demonstrated significant differences between control and Cav-1$^{-/-}$ mice as regarding the NK1r and SP positivity, being the former increased twice and the latter reduced half as much (Fig. 3A and C). NK2r reactivity was higher than in controls, but the difference was not statistically significant (Fig. 3B).

Electron microscopy

In control tissue, SMC and ICC were rich in typical flask-shaped caveolae, 40–60 nm in diameter, frequently opened on the plasma membrane (Fig. 4A–D). In the Cav-1$^{-/-}$ mice (Figs 5 and 6), the overall structure of the tissue was similar to controls but discrete ultrastructural abnormalities were present. Gap junctions between SMC and ICC (Fig. 5C) and between SMC (Fig. 6A) were present as well as the close contacts between ICC and nerve endings (Fig. 5C). Neuronal perikarya and nerve fibres appeared normal (Fig. 5C).

The most important ultrastructural abnormalities were seen in the SMC and ICC. One of these was the absence of the typical caveolae and the presence of large (150–200 nm in diameter) flask-shaped vesicles close to or opened on the plasmalemma (Figs 5A and 6A, C and D). These structures were very few, 195 in 185 SMC profiles (about 1 for each SMC profile) and 34 in 63 ICC profiles (0.5 for each ICC profile). We named them *large-sized caveolae* because opening on the plasma membrane and showing the same shape of the typical caveolae (Fig. 4A–D). The SER cisternae were still present nearby the plasmalemma but showed few contacts with the large-sized caveolae (Fig. 6C and D). Another striking feature consisted in an extraordinary richness in mitochondria in SMC and ICC from Cav-1$^{-/-}$ mice. These organelles, however, had the same morphology and size of the control ones. In the ICC, they filled the entire cytoplasm (Fig. 5A–C) and in the SMC were clustered in paranuclear regions (Fig. 6B).

Cells with the features of telocytes [53] (formerly called interstitial Cajal-like cells, ICLC [54]) were frequently seen at the submucosal border of the circular muscle layer. As previously described for the myocardial ones [55], the characteristic caveolae were not observed in intestinal telocytes from the Cav-1$^{-/-}$ mice but large-sized caveolae were occasionally seen opening on their plasmalemma (Fig. 5D), similarly to ICC and SMC.
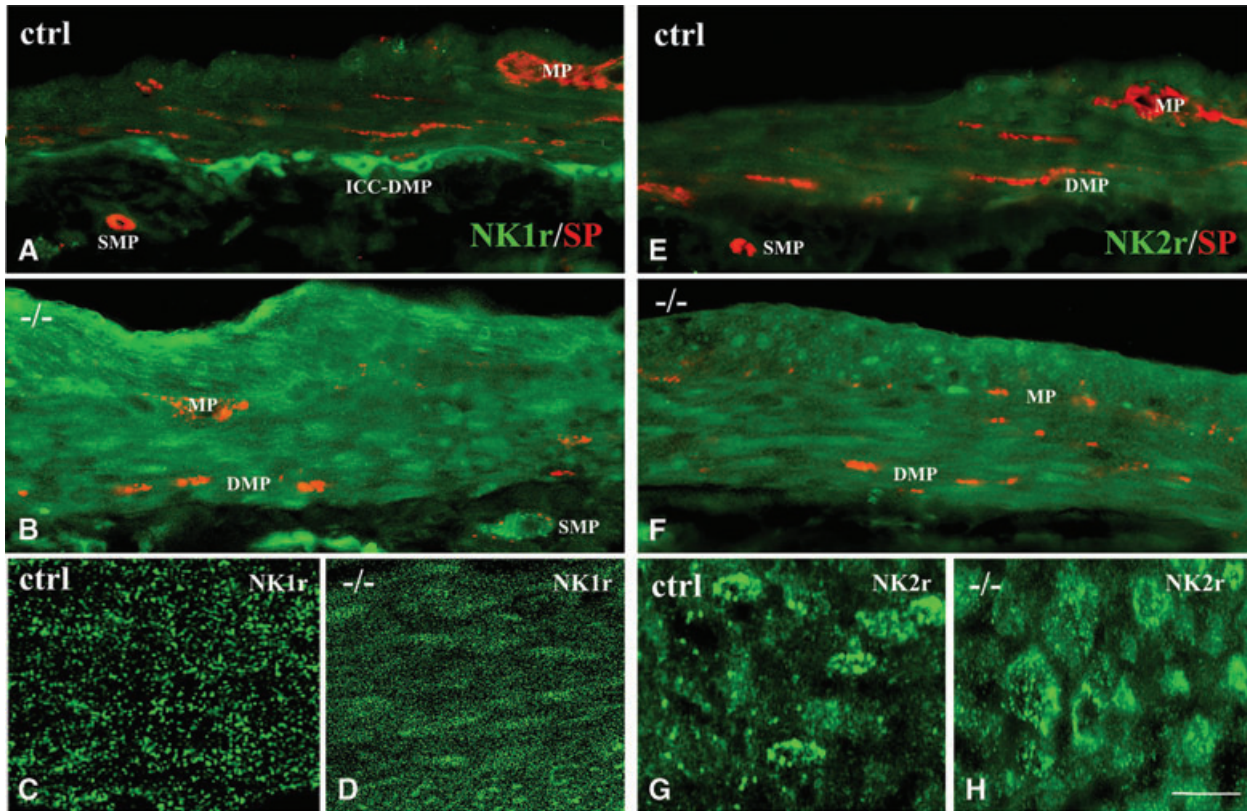
Fig. 2 (A–D) NK1r-IR. In the control, the labelling is intense on the ICC (**A**) and in the smooth muscle cells is on granules mainly distributed on the cell surface (**C**). In the Cav-1$^{-/-}$ mice (**B, D**), the labelling is more intense (**B**) and mainly internalized in the cytoplasm (**D**). (**E–H**) NK2r-IR. The smooth muscle cells are labelled both in control (**E, G**) and Cav-1$^{-/-}$ mice (**F, H**). In the Cav-1$^{-/-}$ mice, the labelling is more intense (**F**) and internalized in the cytoplasm (**H**). (**A, B, E, F**) SP-IR. Labelling is detectable on myenteric and submucous neurons and on intragangliar and intramuscular varicose nerve fibres. In the Cav-1$^{-/-}$ mice (**B, F**), the labelled structures had the same distribution as in controls (**A, E**), although being less numerous. ICC-DMP: Interstitial cells of Cajal at the deep muscular plexus; MP: myenteric plexus; SMP: submucous plexus; DMP: deep muscular plexus. (**A, B, E, F**) Bar = 40 μm and (**C, D, H, G**) Bar = 10 μm.

Discussion

The present immunohistochemical and ultrastructural study demonstrates that the absence of Cav-1 in the mouse small intestine associates with important changes at the level of the ICC, SMC and tachykinergic innervation. The obtained results are in agreement with the previous physiological findings that showed an impaired contractile activity in these animals [33, 34, 38–40].

According to the literature [15, 33, 34, 37–40, 55, 56], Cav-1 and caveolae should be absent in the Cav-1$^{-/-}$ mice. However, under bright field microscope (but not under fluorescent microscope) we observed a faint Cav-1 positivity in these animals. This might be simply an artefact, although a residual Cav-1 transcription cannot be excluded. Indeed, under TEM, caveolae with the characteristic 40–60 nm in diameter were no more identifiable also in our specimens, but we could observe, at very low frequency (in mean, no more than 1 per cell profile), flask-shaped

vesicles with a diameter ranging from 150 to 200 nm close to the plasmalemma of SMC, ICC and telocytes. We considered these structures as large-sized caveolae and they could represent an attempt to compensate the loss of the normal-sized caveolae. These large-sized caveolae had few of the nanocontacts with SER cisternae and mitochondria reported for the SMC [17–20], even though the latter organelles where increased in number compared with controls. This datum is very important because caveolae represent an extracellular source of calcium by which SER restores its normal calcium level [15, 34, 38].

There are considerable evidences that a loss of signalling molecules accompanies that of caveolae [15, 33, 34, 38] and this loss results in an impairment of contractile activity and reduced pacing frequencies in the gut of Cav-1$^{-/-}$ mice [34, 38, 39]. In our specimens from Cav-1$^{-/-}$ mice, the ICC, although still c-kit-IR, are no more Ano1-IR. The Ano-1 is a calcium-activated chloride channel involved in sensory signal transduction and smooth muscle
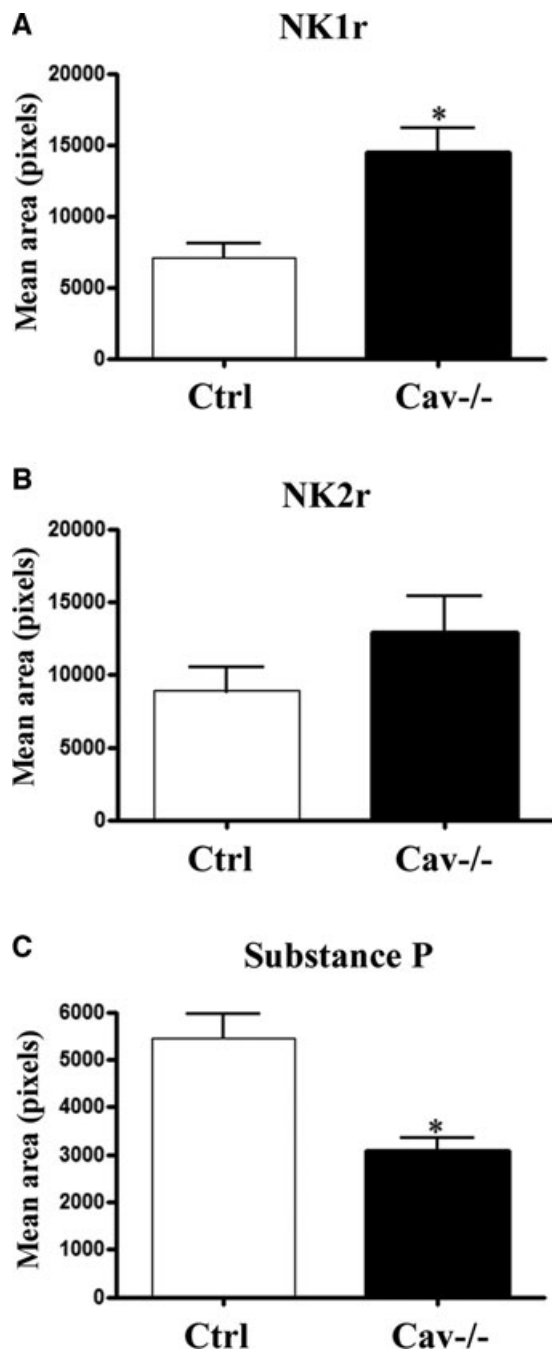
A

NK1r

B

NK2r

C

Substance P

Fig. 3 Quantification of the NKr-IR and SP-IR in the intestinal muscle coat of control (white column) and Cav$^{-/-}$ (black column) mice. (**A**, **B**) NK1r-IR and NK2r-IR are higher in the mutant mice compared to controls, although only the NK1r-IR increase is statistically significant. (**C**) SP-IR is significantly lower in the mutant mice compared to controls. *$P < 0.01$ compared to control mice.

contraction [45] and required for the rhythmic contractions of the intestinal smooth muscle [42–44]. Its absence gets well along

with the reduced pacing frequencies recorded in the small intestine of Cav-1$^{-/-}$ mice.

The extraordinary richness in mitochondria we found by TEM examination in both ICC and SMC of the Cav-1$^{-/-}$ mice is an unexpected and striking feature. Several studies underlie the importance of mitochondria in modulating cytosolic calcium signalling [57–60]. The presence of so many mitochondria might be an attempt, likely acting as Ca^{2+} buffer, to compensate the defect in cytosolic calcium concentration and the calcium signalling molecules loss due to caveolae absence. Besides, an increased production of ATP could be an alternative way in the maintenance of contraction.

According to the available data, the loss of Cav-1 or the disruption of caveolae in the mouse intestine does not affect either the cholinergic or the nitrergic innervation [40, 41]. However, a defective response to nitric oxide and ACh release was observed [40, 41], suggesting the presence of a post-junctional defect. Interestingly, the present data indicate that the excitatory tachykinergic (SP-IR) neurons are compromised in the Cav-1$^{-/-}$ mice, because a statistically significant reduction in the SP-IR was observed. The reduced contractility characterizing these animals is in agreement with the decrease in SP content but in contrast with the significant increase and intracytoplasmic distribution (internalization) of the NKr in the SMC. However, this discrepancy might be explained with the occurrence of a first change at the NK receptor location, likely due to Cav-1 loss, then followed by a decrease in SP production.

In conclusion, this study shows important and not yet reported changes in SMC, ICC, neurons and telocytes of the Cav-1$^{-/-}$ mice and emphasizes the complexity of molecular mechanisms controlling the intestinal motility. Loss of Ano1 expression in the ICC and rearrangement of NK receptors in the SMC are interpretable as consequence of Cav-1/caveolae loss and possibly responsible for the impaired contractile activity. To note, despite the reported involvement of several organs, the Cav-1$^{-/-}$ mice are viable. In this respect, the impressive richness in mitochondria and the decrease in SP content we found in these animals might represent the ways to compensate the reduced calcium availability and the increased expression of NKr, thus allowing the maintenance of a certain cell function.

Acknowledgements

Conflict of interest

The authors confirm that there are no conflicts of interest.

Fig. 4 Electron microscopy. Control mice. In (**A**), Interstitial cells of Cajal (ICC) at the deep muscular plexus and in (**B**) at the myenteric plexus. All ICC are rich in mitochondria and caveolae. Details of the caveolae of the smooth muscle cells in (**C**), and of one nexus (asterisk) between two smooth muscle cells (SMC) in (**D**). NE: nerve endings; cap: blood capillary; SMC: smooth muscle cells. (**A**) Bar = 1.5 μm; (**B**) Bar = 2.0 μm; (**C**) Bar = 0.4 μm and (**D**) Bar = 0.33 μm.
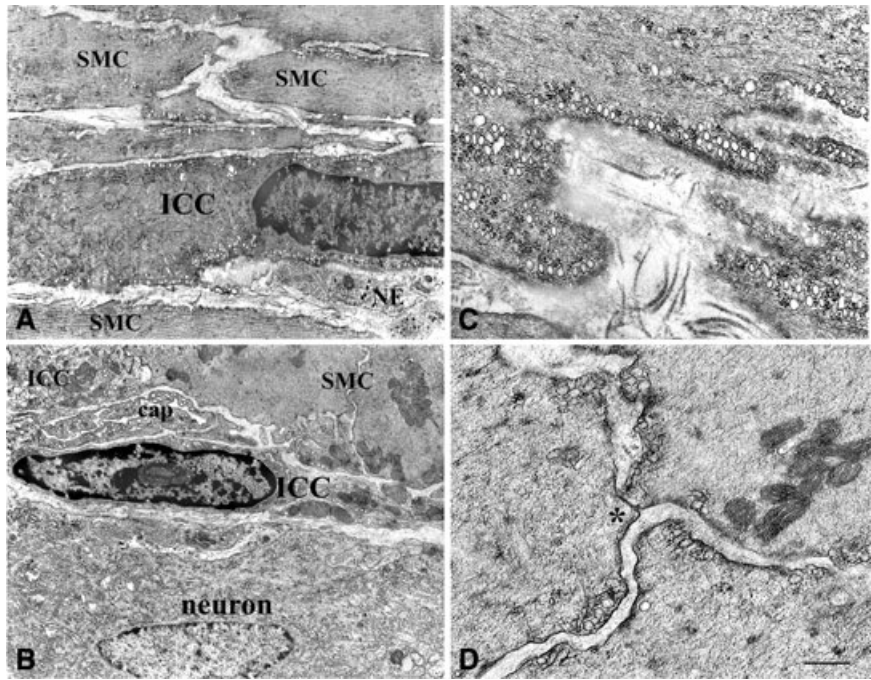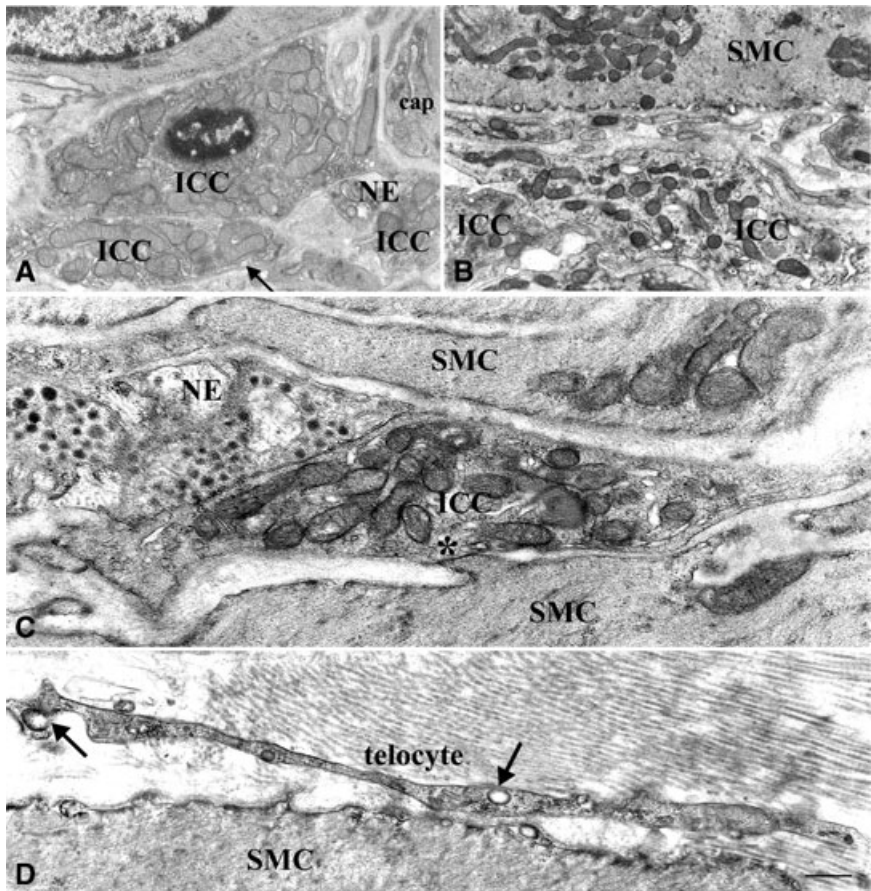

Fig. 5 Electron microscopy. Cav-1$^{-/-}$ mice. (**A–C**) Interstitial cells of Cajal, in (**A**) and (**C**), at the deep muscular plexus and in (**B**) at the myenteric plexus. All these cells are extraordinary rich in mitochondria. In (**C**), a gap junction* between one smooth muscle cell (SMC) and one interstitial cell. The latter is also in close contact with nerve endings (NE). (**D**) A telocyte located at the submucosal border of the circular muscle layer. SMC: smooth muscle cells; NE: nerve endings; ICC: interstitial cells of Cajal. The arrows indicate the large-sized caveolae. (**A**) Bar = 2.0 μm; (**B**) Bar = 4.0 μm and (**C** and **D**) Bar = 0.4 μm.
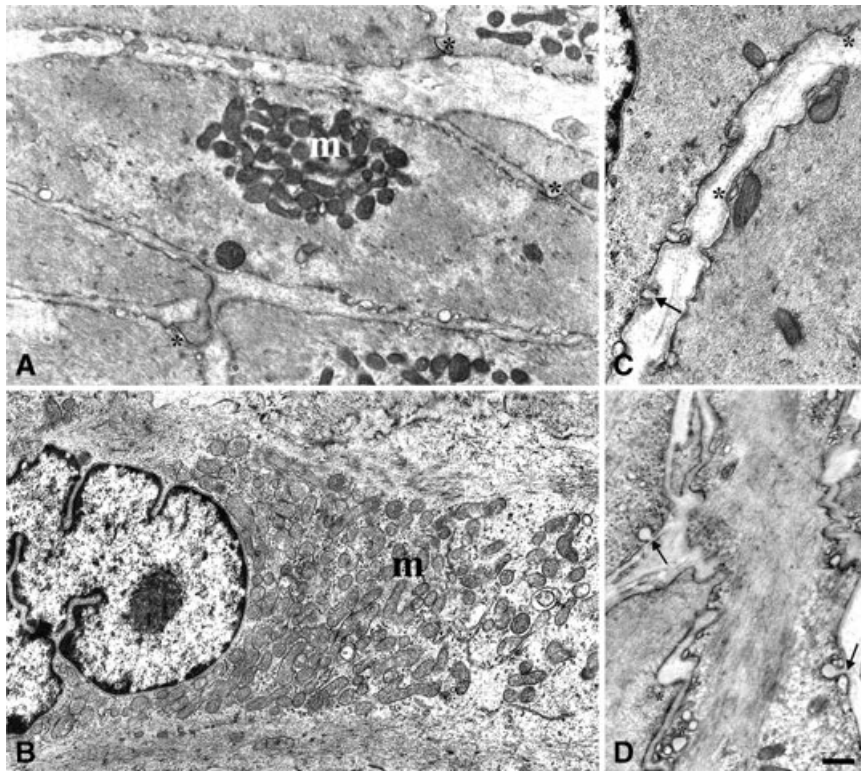
Fig. 6 Electron microscopy. Cav-1$^{-/-}$ mice. (**A–D**) Smooth muscle cells. All smooth muscle cells, both the circular (**A**) and longitudinal ones (**B**), are particularly rich in mitochondria (m). Gap junctions are maintained (asterisks in **A**) as well as the cisternae of the smooth endoplasmic reticulum (asterisks in **C**). The arrows in (**C**) and (**D**) indicate large-sized caveolae opening on the cell surface. (**A**) Bar = 1.0 μm; (**B**) Bar = 0.8 μm; (**C**) Bar = 0.5 μm and (**D**) Bar = 0.8 μm.

References

1. **Palade GE.** Fine structure of blood capillaries. *J Appl Physiol.* 1953; 24: 1424–36.
2. **Anderson RGW.** The caveolae membrane system. *Annu Rev Biochem.* 1998; 67: 199–225.
3. **Ostrom RS, Insel PA.** Caveolar microdomains of the sarcolemma: compartmentation of signaling molecules comes of age. *Circ Res.* 1999; 84: 1110–2.
4. **Razani B, Woodman SE, Lisanti MP.** Caveolae: from cell biology to animal physiology. *Pharmacol Rev.* 2002; 54:431–67.
5. **Faussone-Pellegrini MS, Cortesini C, et al.** Sull'ultrastruttura della tunica muscolare della porzione cardiale dell'esofago e dello stomaco umano con particolare riferimento alle cosidette cellule interstiziali del Cajal. *Arch It Anat Embriol.* 1977; 82:157–77.
6. **Thuneberg L.** Interstitial cells of Cajal: intestinal pacemaker cells? *Adv Anat Embryol Cell Biol.* 1982; 71: 1–130.
7. **Faussone-Pellegrini MS.** Comparative study of interstitial cells of Cajal. *Acta Anat.* 1987; 130: 109–26.
8. **Faussone-Pellegrini MS.** Histogenesis, structure and relationships of interstitial cells of Cajal (ICC): from morphology to functional interpretation. *Eur J Morphol.* 1992; 30: 37–48.
9. **Faussone-Pellegrini MS.** Interstitial cells of Cajal: once negligible players, now blazing protagonists. *Ital J Anat Embryol.* 2005; 110: 11–31.
10. **Gabella G.** Caveolae intracellulares and sarcoplasmic reticulum in smooth muscle. *J Cell Sci.* 1971; 8: 601–9.
11. **Popescu LM, Diculescu I, Zelck U, et al.** Ultrastructural distribution of calcium in smooth-muscle cells of guinea-pig *Taenia coli*-correlated electron-microscopic and quantitative study. *Cell Tiss Res.* 1974; 154: 357–78.
12. **Popescu LM.** Conceptual model of the excitation-contraction coupling in smooth muscle; the possible role of the surface microvesicles. *Studia Biophys. (Berlin).* 1974; 44: S141–53.
13. **Popescu LM, Diculescu I.** Calcium in smooth muscle sarcoplasmic reticulum *in situ.* Conventional and X-ray analytical electron microscopy. *J Cell Biol.* 1975; 67: 911–8.
14. **Isshiki M, Anderson RGW.** Function of caveolae in Ca^{2+} entry and Ca^{2+}-dependent signal transduction. *Traffic* 2003; 4: 717–23.
15. **Daniel EE, El-Yazbi AF, Cho WJ.** Caveolae and calcium handling: a review and a hypothesis. *J Cell Mol Med.* 2006; 10: 529–44.
16. **Bolton TB.** Calcium events in smooth muscles and their interstitial cells; physiological roles of sparks. *J Physiol.* 2006; 570: 5–11
17. **Poburko D, Kuo KH, Dai J, et al.** Organellar junctions promote targeted Ca^{2+} signaling in smooth muscle: why two membranes are better than one. *Trends Pharmacol Sci.* 2004; 25: 8–15.
18. **Gherghiceanu M, Popescu LM.** Caveolar nanospaces in smooth muscle cells. *J Cell Mol Med.* 2006; 10: 519–28.
19. **Popescu LM, Gherghiceanu M, Mandache E, et al.** Caveolae in smooth

muscles: nanocontacts. *J Cell Mol Med*. 2006; 10: 960–90.

20. **Gherghiceanu M, Popescu LM.** Electron microscope tomography: further demonstration of nanocontacts between caveolae and smooth muscle sarcoplasmic reticulum. *J Cell Mol Med*. 2007; 10: 1416–8.

21. **Simionescu N, Simionescu M, Palade GE.** Permeability of muscle capillaries to small heme-peptides. Evidence for the existence of patent transendothelial channels. *J Cell Biol*. 1975; 64: 586–607.

22. **Predescu SA, Predescu DN, Palade GE.** Endothelial transcytotic machinery involves supramolecular protein-lipid complexes. *Mol Biol Cell*. 2001; 12: 1019–33.

23. **Anderson RG, Kamen BA, Rothberg KG, et al.** Potocytosis: sequestration and transport of small molecules by caveolae. *Science* 1992; 255: 410–1.

24. **Anderson RG.** Potocytosis of small molecules and ions by caveolae. *Trends Cell Biol*. 1993; 3: 69–72.

25. **Anderson HA, Chen Y, Norkin LC.** Bound simian virus 40 translocates to caveolin enriched membrane domains, and its entry is inhibited by drugs and selectively disrupts caveolae. *Mol Biol Cell*. 1996; 7: 8–25.

26. **Stang E, Kartenbeck J, Parton RG.** Major histocompatibility complex class I molecules mediate association of SV40 with caveolae. *Mol Biol Cell*. 1997; 8: 47–57.

27. **Pelkmans L, Kartenbeck J, Helenius A.** Caveolar endocytosis of simian virus 40 reveals a new two-step vesicular-transport pathway to the ER. *Nature Cell Biol*. 2001; 3: 473–83.

28. **Ostrom RS, Insel PA.** Caveolar microdomains of the sarcolemma: compartmentation of signaling molecules comes of age. *Circ Res*. 1999; 84: 1110–2.

29. **Isshiki M, Anderson RG.** Calcium signal transduction from caveolae. *Cell Calcium*. 1999; 26: 201–8.

30. **Shaul PW, Anderson RGW.** Role of plasmalemmal caveolae in signal transduction. *Am J Physiol Lung Cell Mol Physiol*. 1998; 275: 842–51.

31. **Rothberg KG, Heuser JE, Donzell DC, et al.** Caveolin, a protein component of caveolae membrane coats. *Cell*. 1992; 68: 673–82.

32. **Chang WJ, Ying YS, Rothberg KG, et al.** Purification and characterization of smooth muscle cell caveolae. *J Cell Biol*. 1994; 126: 127–38.

33. **Daniel EE, Bodie G, Mannarino M, et al.** Changes in membrane cholesterol affect caveolin-1 localization and ICC-pacing in mouse jejunum. *J Physiol Gastrointest Liver Physiol*. 2004; 287: G202–10.

34. **Daniel EE, Eteraf T, Sommer B, et al.** The role of caveolae and caveolin 1 in calcium handling in pacing and contraction of mouse intestine. *J Cell Mol Med*. 2009; 13: 352–64.

35. **Sargiacomo M, Scherer PE, Tang Z, et al.** Oligomeris structure of caveolin: implications for caveolae membrane organization. *Proc Natl Acad Sci U.S.A.* 1995; 92: 9407–11.

36. **Krajewska WM, Masłowska I.** Caveolins: structure and function in signal transduction. *Cell Mol Biol Lett*. 2004; 9: 195–220.

37. **Cho WJ, Daniel EE.** Proteins of interstitial cells of Cajal and intestinal smooth muscle co-localized with caveolin-1. *Am J Physiol Gastrointest Liver Physiol*. 2005; 288: G571–85.

38. **El-Yazbi AF, Cho WJ, Schulz R, et al.** Calcium extrusion by plasma membrane calcium pump is impaired in caveolin-1 knockout mouse small intestine. *Eur J Pharmacol*. 2008; 591: 80–7.

39. **El-Yazbi AF, Cho WJ, Schulz R, et al.** Caveolin-1 knockout alters beta-adrenoceptors function in mouse small intestine. *Am J Physiol Gastrointest Liver Physiol*. 2006; 291: G1020–30.

40. **El-Yazbi AF, Cho WJ, Boddy G, et al.** Caveolin-1 gene knockout impairs nitrergic function in mouse small intestine. *Brit J Pharmacol*. 2005; 145: 1017–26.

41. **El-Yazbi AF, Cho WJ, Cena J, et al.** Smooth muscle NOS, colocalized with caveolin-1, modulates contraction in mouse small intestine. *J Cell Mol Med*. 2008; 12: 1404–15.

42. **Huang F, Rock JR, Harfe BD, et al.** Studies on expression and function of the TMEM16A calcium-activated chloride channel. *Proc Natl Acad Sci U.S.A.* 2009; 106: 21413–8.

43. **Gomez-Pinilla PJ, Gibbons SJ, Bardsley MR, et al.** Ano1 is a selective marker of interstitial cells of Cajal in the human and mouse gastrointestinal tract. *Am J Physiol Gastrointest Liver Physiol*. 2009; 296: G1370–81.

44. **Hwang SJ, Blair PJ, Britton FC, et al.** Expression of anoctamin 1/TMEM16A by interstitial cells of Cajal is fundamental for slow wave activity in gastrointestinal muscles. *J Physiol*. 2009; 587: 4887–904.

45. **Caputo A, Caci E, Ferrera L, et al.** TMEM16A, a membrane protein associated with calcium-dependent chloride channel activity. *Science*. 2008; 322: 590–4.

46. **Vannucchi MG, Corsani L, Bani D, et al.** Myenteric neurons and interstitial cells of Cajal of mouse colon express several nitric oxide synthase isoforms. *Neurosci Lett*. 2002; 326: 191–5.

47. **Mulè F, Vannucchi MG, Corsani L, et al.** Myogenic NOS and endogenous NO production are defective in colon from dystrophic (mdx) mice. *Am J Physiol Gastrointest Liver Physiol*. 2001; 281: G1264–70.

48. **Vannucchi MG, Zizzo G, Zardo C, et al.** Ultrastructural changes in the interstitial cells of Cajal and gastric dysrhythmias in mice lacking full-length dystrophin (*mdx* mice). *J Cell Physiol*. 2004; 199: 293–309.

49. **Amato A, Vannucchi MG, Faussone-Pellegrini MS, et al.** Altered tachykinergic influence on gastric mechanical activity in *mdx* mice. *Neurogastroenterol Mot*. 2006; 18: 844–52.

50. **Faussone-Pellegrini MS, Vannucchi MG.** Substance P and Neurokinin 1 receptor-expression is affected in the ileum of mice with mutation in the W locus. *J Cell Mol Med*. 2006; 10: 511–8.

51. **Vigna SR, Bowden JJ, McDonald DM, et al.** Characterization of antibodies to the rat substance P (NK1) receptor and to a chimeric substance P receptor expressed in mammalian cells. *J Neurosci*. 1994; 14: 834–45.

52. **Grady EF, Baluk P, Bohm S, et al.** Characterization of antisera specific to NK1, NK2, and NK3 neurokinin receptors and their utilization to localize receptors in the rat gastrointestinal tract. *J Neurosci*. 1996; 16: 6975–86.

53. **Popescu LM, Faussone-Pellegrini MS.** TELOCYTES-a case of serendipity: the winding way from Interstitial Cells of Cajal (ICC), *via* Interstitial Cajal-Like Cells (ICLC) to TELOCYTES. *J Cell Mol Med*. 2010; 14: 729–40.

54. **Pieri L, Vannucchi MG, Faussone-Pellegrini MS.** Histochemical and ultrastructural characteristics of an interstitial cell type different from ICC and resident in the muscle coat of human gut. *J Cell Mol Med*. 2008; 12: 1944–55.

55. **Gherghiceanu M, Hinescu ME, Popescu LM.** Myocardial interstitial Cajal-like cells (ICLC) in caveolin-1 KO mice. *J Cell Mol Med*. 2009; 13: 202–6.

56. **Shakirova Y, Bonnevier J, Albinsson S, et al.** Increased Rho activation and

PKC-mediated smooth muscle contractility in the absence of caveolin-1. *Am J Physiol Cell Physiol.* 2006; 291: C1326–35.

57. **Babcock DF, Herrington J, Goodwin PC, *et al*.** Mitochondrial participation in the intracellular Ca^{2+} network. *J Cell Biol.* 1997; 136: 833–44.

58. **Hoth M, Fanger CM, Lewis RS.** Mitochondrial regulation of store-operated calcium signaling in T lymphocytes. *J Cell Biol*. 1997; 137: 633–48.

59. **Brini M.** Ca^{2+} signalling in mitochondria: mechanism and role in physiology and pathology. *Cell Calcium.* 2003; 34: 399–405.

60. **Collins S, Meyer T.** A sensor for calcium uptake. *Nature.* 2010; 467: 283.